ELSEVIER

Carbohydrate Research 262 (1994) 27–47

CARBOHYDRATE RESEARCH

Cellulose char structure: a combined analytical Py–GC–MS, FTIR, and NMR study

Ivana Pastorova [a,*], Robert E. Botto [b], Peter W. Arisz [a], Jaap J. Boon [a]

[a] *Unit for Mass Spectrometry of Macromolecular Systems, FOM Institute for Atomic and Molecular Physics, Kruislaan 407, 1098 SJ Amsterdam, Netherlands*

[b] *Chemistry Division, Argonne National Laboratory, 9700 South Cass Avenue, Argonne, IL 60439, USA*

Received 24 January 1994; accepted 30 March 1994

Abstract

Bulk samples of microcrystalline cellulose were charred in an anaerobic environment, at atmospheric pressure, and temperatures ranging from 190 to 390°C. Curie-point pyrolysis–gas chromatography–mass spectrometry (Cu-Py–GC–MS) was used as an analytical tool for characterization of the resulting chars. Fourier-transform infrared (FTIR) spectroscopy and solid-state ^{13}C nuclear magnetic resonance (NMR) spectroscopy were employed for verification of the results. The abundance of aromatic building blocks (furans, alkylbenzenes, and alkylnaphthalenes) in Cu-Py–GC chromatograms increases with the pretreatment temperature. FTIR and NMR show the breakdown of the pyranose polymer and gradual formation of a new intermediate polymer with an aromatic character which disproportionates further and aromatizes at temperatures above 310°C. A model for the formation of this intermediate polymer is proposed. Cu-Py–GC–MS data are in agreement with the results of FTIR and NMR.

Key words: Cellulose char structure; Combined analytical Py–GC–MS, FTIR, and NMR

1. Introduction

Cellulose is the major component of the cell walls of vascular plants, and considerable attention has been focused on the thermal decomposition of this biopolymer [1]. A vast amount of information is available on cellulose pyrolysis

* Corresponding author.

SSDI 0008-6215(94)00120-5

[2–6]; however, only a few of the reactions occurring during this process are well understood.

Pyrolysis of cellulose typically results in a distribution of solid, liquid, and gaseous products. The latter two are of commercial interest and their formation has been the subject of extensive research. They are usually produced at higher temperatures (> 300°C), by three competing reaction pathways: transglycosidation, [2 + 2 + 2] cycloreversion, and elimination reactions [1,7].

Considerably less research has been devoted to the study of the nature of the carbonaceous char formed under certain conditions during cellulose pyrolysis [8,9]. The production of char is enhanced by inorganic additives, low pyrolysis temperatures with slow heating rates, and higher pressures [10], but the exact synthetic processes leading to char formation as well as the structure of the char still remain unknown.

There are indications that the charring reactions, in addition to dehydration, involve condensation and decomposition of the condensation products, followed by homolytic elimination of the carbon substituents [11]. ESR, within the range of 70–280°C, suggested that the initial reactions are heterolytic, but charring above 200°C involves the formation of stable free radicals [5]. Some of them stay trapped in the matrix, some of them result in interlinking of the carbon chain and further dehydration to a carbonaceous residue.

The studies of cellulose samples of increasing thickness implied the formation of a secondary char resulting from the decomposition of volatile matter (levoglucosan), which was unable to rapidly escape from the thicker cellulose samples [13].

Slow heating, low temperature cellulose chars were described in our earlier work [14,15]. These chars were prepared in order to simulate polysaccharide char formation in charred archaeological food residues. It appears that charring of the food residues has a positive effect on preservation of some biomolecular markers. The process or mechanism responsible for the preservation of these biomolecular markers still remains unknown [16,17], but they seem to be grafted onto chars from polysaccharides.

The study of model cellulose chars by Py–CIMS and by HPLC of derivatised off-line Cu-Py condensates [14] shows that glucose oligosaccharides retaining the original β-(1 → 4)-glycosidic linkage are preserved in cellulose chars up to the relatively high temperature of 270°C. At the same time, heating of cellulose results in the formation of a characteristic condensed black char, as has been shown by a discriminant analysis of Py–EIMS data [15]. It was proposed that the characteristic higher mass fraction in the Py–EIMS spectra of the experimental cellulose chars represents one or more homologous series of aromatic compounds. This characteristic higher mass fraction was present in Py–EIMS spectrum of an acid hydrolysis residue of cellulose heated for 2.5 h at 250°C. Therefore, 250°C seems to be the minimum temperature needed for char formation under the selected experimental conditions (anoxic environment, atmospheric pressure, and a constant flow of nitrogen) [15].

From all this data, it is still difficult to propose a mechanism for cellulose char formation, as a second, analytical pyrolysis is involved in the study of already

pyrolysed samples. In this work, Py–GC–MS is used as an analytical tool for a set of experimental cellulose chars and FTIR and solid-state ^{13}C NMR are employed for verification of the results. Both these techniques are widely used instrumental methods by cellulose chemists for investigating physical and chemical properties [18,19]. FTIR has been applied before to study hydrogen bonding, degradation and decomposition processes, and chemical modifications of cellulose [20]. By combining the results of these analytical methods it is possible to get a more complete picture of the processes leading to the formation of char from cellulose.

2. Experimental

Preparation of cellulose chars.—The conditions used for the preparation of the model polysaccharide chars are different from those used for artificial coalification as well as from those used generally in pyrolysis of cellulose. Our rationale for this approach has been described before [15].

Microcrystalline cellulose (ca. 0.5 g; Cellulose microcrystalline Avicel for thin layer chromatography, E. Merck, Germany) was placed in a glass tube with a sinter and continuously flushed with N_2 at a flow rate of 80 mL/min during the whole reaction time [14]. The tube was inserted in a preheated oven. The tube with the sample was weighed before and after heating, in order to determine the relative weight loss. The heating time for all samples was 150 min. The temperatures used for preparation of the primary chars were 190, 220, 250, 270, 290, 310, 350, and 390°C, respectively, and produced samples coded char 190, char 220, char 250, char 270, char 290, char 310, char 350, and char 390. Gases and volatiles were vented.

Curie-point pyrolysis–gas chromatography–mass spectrometry.—Pyrolysis–gas chromatography–mass spectrometry was performed with a Hewlett–Packard 5890 series II GC, equipped with a FOM-4LX pyrolysis unit and coupled with a Finnigan MAT INCOS 50 mass spectrometer and Data General 10 Computer for acquisition. The pyrolysis conditions were as follows: Curie-point t 610°C, 770°C, t rise time 0.1 s (200°C/s), total pyrolysis time 4.0 s, and t of the pyrolysis chamber 180°C. The unit was flushed with He, which was also used as the carrier gas, with a constant linear flow velocity of 27 cm/min. The pyrolysate was directly introduced into a capillary column [25-m CP Sil 5 CB fused silica capillary column (i.d., 0.22 mm; film thickness, 1.4 μm; Chrompack)]. The GC oven was kept at 5°C during and for 3 min after pyrolysis, and subsequently heated to 222°C at 6°C/min and then to 300°C at 15°C/min. Compounds were ionized at 70 eV (EI conditions).

Nuclear magnetic resonance and infrared spectroscopy.—Solid-state ^{13}C NMR spectra were obtained at 25.18 MHz on a Bruker CXP-100 (2.3 Tesla) spectrometer equipped with a doubly-tuned, single-coil probe and a dual air-bearing spinning apparatus. Ceramic rotors, with an internal volume of 250 μL, were packed with cellulose char and spun at ca. 4 kHz. Cross-polarization (CP) experiments were performed using a contact time of 1.5 ms and a 1-s pulse repetition time, a 56-kHz proton decoupling field (4.25-μs 90° pulse width), a spectral width of 10 kHz, and an acquisition time of 20 ms. Between 4000–8000 transients were obtained for

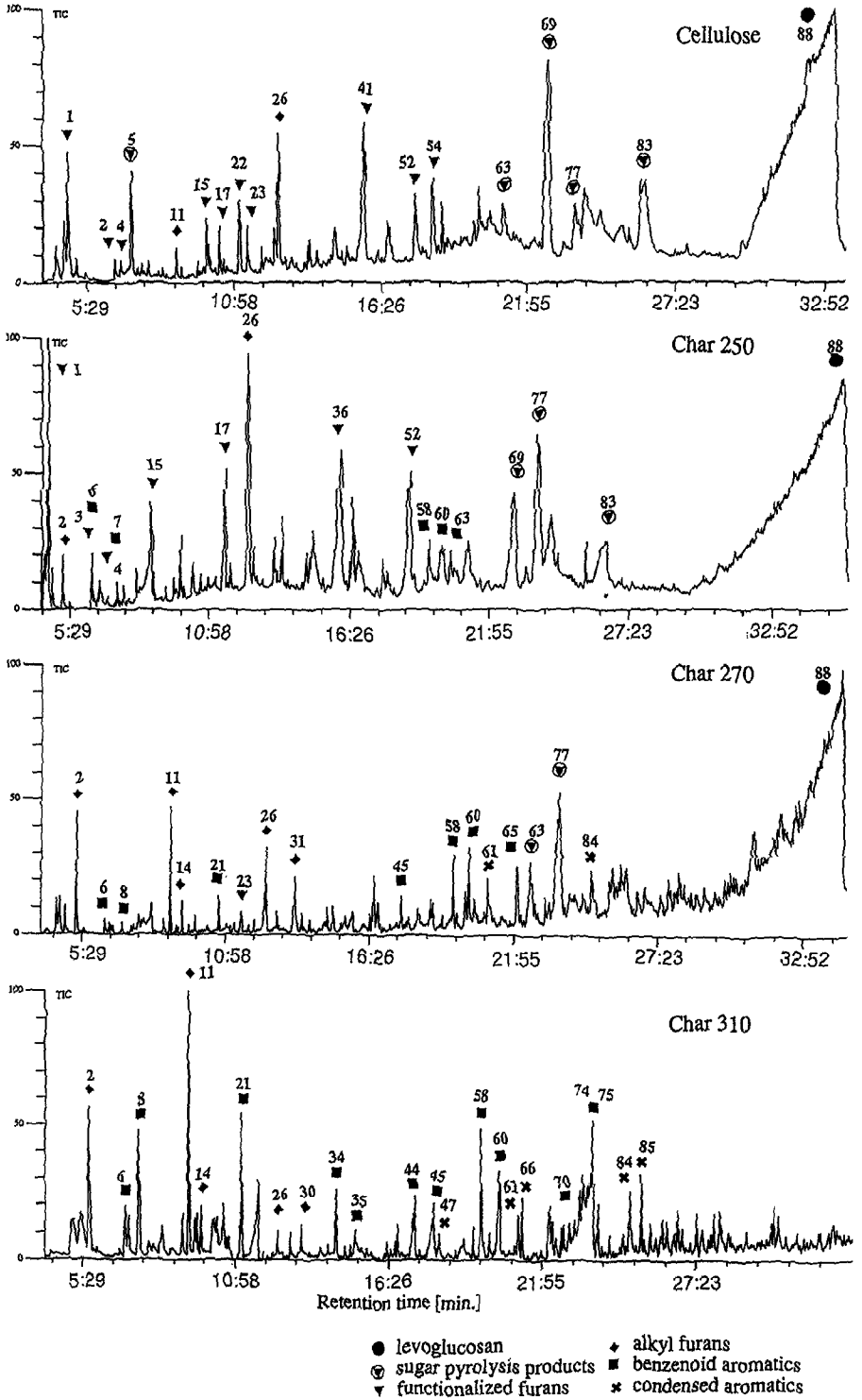

Fig. 1. Gas chromatograms as TICs from GC–MS data of 610°C Curie point pyrolysates of cellulose and cellulose chars 250, 270, and 310.

each sample. In a typical experiment, a memory of 200 words was allocated for data acquisition and it was then increased to 4K (2K real data) by zero filling. Before Fourier transformation of the data, the interferogram was multiplied by a decreasing trapezoidal window function after the first 100 data points for cellulose, and after the first 40 data points for char samples. Chemical shifts are referenced in parts per million (ppm) from Me_4Si using tetrakis(trimethylsilyl)silane as a secondary reference [21].

Fourier-transform infrared (FTIR) spectroscopy was performed on a Nicolet 510P spectrometer using the diffuse reflectance method; the instrument resolution was 2 cm^{-1}.

3. Results

Curie-point–pyrolysis–gas chromatography–mass spectrometry.—Two Curie-point temperatures were used, 610°C for samples char 190 to char 310 and 770°C for char 270 to char 390. Lists of identified compounds are shown in Table 1 and 2.

Chars 190 and 220 (not shown) have a very similar distribution of pyrolysis products that are typical of microcrystalline cellulose. Cu–Py–GC–MS of these two low temperature chars revealed mostly pyranones, furanones, and furans, besides the main product, levoglucosan. All the identified compounds have been detected previously in pyrolysates of microcrystalline cellulose [22] (Fig. 1).

In the chromatogram of char 250, the relative ratios between individual pyrolysis products changes. Several products appear that have not been identified previously in simple, noncatalysed cellulose pyrolysates, such as cyclohexadienes, vinylfuran, 2-*n*-propylfuran. Also, benzene and phenol derivatives (e.g., dimethylbenzenes and methylphenols) contribute more significantly to the pyrolysis products than found for native cellulose [22].

This phenomenon becomes even more evident in the Py–GC chromatograms of chars 270 and 290 (not shown). Here, the "classical" pyrolysis products of microcrystalline cellulose are present together with a wide range of aromatic compounds, as well as condensed aromatic compounds such as benzofurans and naphthalenes. From Table 1 and Fig. 1, it is evident that the aromatic components of the pyrolysate of char 310 become more abundant than the oxygen-containing saturated compounds.

Table 2 shows a list of compounds identified in Py–GC chromatograms of chars 290, 310, 350, and 390 with a higher Curie-point temperature (t_{cp}) of 770°C. Chars 290 and 310 were measured in order to assess the influence of a higher t_{cp} on the product distribution. Clear differences can be seen from Table 2 and Fig. 2. They are the result of two processes. Some compounds, especially anhydrohexoses, pyranones, and furanones, decompose at this higher temperature and form lower molecular weight compounds that are thermodynamically more stable, such as furan or methylfurans. The second process is the release of even more aromatic species resulting from the breakdown of bonds with high dissociation energies, analogous with the pyrolysis of coals [23].

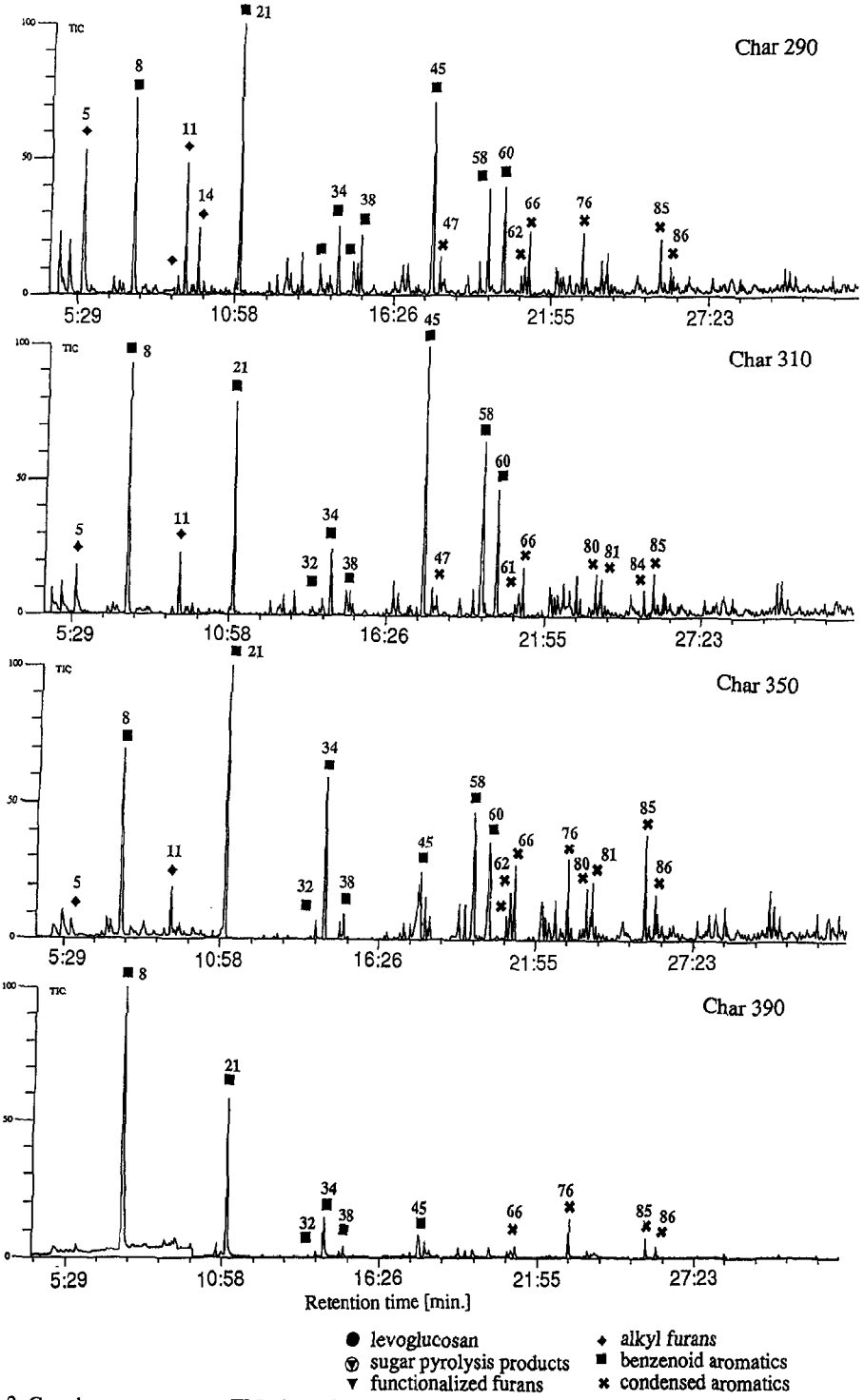

Fig. 2. Gas chromatograms as TICs from GC–MS data of 770°C Curie point pyrolysates of cellulose and cellulose chars 290, 310, 350, and 390.

Py–GC data for chars 350 and 390 were obtained only at a higher t_{cp} because of their inert behaviour at lower t_{cp}. This suggests that these higher temperature chars contain more highly condensed, thermally stable structures. Condensed aromatic compounds, such as, benzofurans, dibenzofuran, fluorene, and naphthalene derivatives, were identified among the pyrolysis products of these chars.

For a better illustration of the changes in the distribution of functional groups and the degree of saturation of products for the series of char samples, pyrolysis products were divided into five classes: (A) sugar markers, (B) functionalized furans, (C) alkyl furans, (D) benzenoid aromatics, and (E) condensed aromatics. Representative structures are shown in Fig. 3A–E. Contributions of these classes of compounds to the total product distribution in the Py–GC chromatograms is shown in Fig. 4A and B. The relative amounts of sugar markers decrease with the higher preheating temperatures. The abundance of furans increases slowly in the series of chars until char 290. Thereafter, their abundance decreases again, along with a concomitant increase in the relative amounts of aromatic and condensed aromatic structures.

Fourier transform infrared spectroscopy.—Using FTIR, it is possible to follow the structural and chemical changes in cellulose and gradual formation of cellulose chars with the increasing charring temperature. FTIR spectra are presented in Fig. 5. The FTIR spectrum of microcrystalline cellulose contains several absorption bands, which have been assigned to individual structural units of cellulose as listed in Table 3.

The spectrum of char 220 (not shown) is very similar to that of cellulose. However, the first indication of dehydration is revealed by the lower intensity of the O–H stretching band (3600–3100 cm^{-1}) compared with cellulose, as well as by the decreased intensity of the 990 cm^{-1} band for C–O skeletal vibrations of secondary alcohols. At 1620 and 1700 cm^{-1}, two new bands begin to appear. These have been assigned to C = C and C = O stretching frequencies, respectively. These vibrations are even more pronounced in the spectrum of char 250, although it is evident that most of the pyranose structures of cellulose are still preserved (C–O stretching in pyranose ring at 1200 cm^{-1} and C–O–C skeletal vibrations at 1080 cm^{-1}).

Char 270 has been severely dehydrated; very little of the pyranose character is preserved. Also, the C = C and C = O stretching absorption bands at 1620 and 1700 cm^{-1} become very strong. Greater dehydration and increased aromatization are observed in the spectrum of char 290 (not shown). Absorbances in the 1000–800 cm^{-1} region (aromatic out of plane bending) imply that there are some aromatic structures present in this solid residue. In char 310, aromatic compounds become even more prevalent. Absorbances in the 1500–1000 cm^{-1} region can be attributed to aromatic C = C skeletal vibrations (1450 cm^{-1}) and C–H deformation modes in alkenes. Further loss of oxygen from the char is reflected in the change in the ratio between intensities assigned to C = O and C = C stretching modes. The intensity of the peak with a maximum at 1700 cm^{-1} (C = O str.) decreases accordingly.

The oxygen contents for chars 350 (not shown) and 390 decrease even further,

Table 1
Identified compounds in the Cu(610°C)-Py–GC–MS data of microcrystalline cellulose (1), char 190 (2), char 250 (3), char 270 (4), char 290 (5), and char 310 (6). The numbering of the compounds corresponds with Fig. 1

No.	Class	MW [a]	Compound [b]	Sample				
				1	2	3	4	5
1	A	86	2,3-Butanedione	+	+	+	–	–
2	A	70	2-Butenal (*cis*)	+	+	+	–	–
3	A	70	2-Butenal (*trans*)	+	+	+	–	–
4	A	74	Hydroxypropanone	–	–	–	–	–
5	C	82	2 or 3-Methylfuran	+	+	+	+	–
6	D	80	1,4-Cyclohexadiene	+	+	+	+	–
7	D	80	1,3-Cyclohexadiene	+	+	+	+	–
8	D	78	Benzene	+	+	+	+	+
9	A	86	Tetrahydrofuran-3-one	–	–	–	–	–
10	C	96	2-Ethylfuran	+	+	+	+	–
11	C	96	2,5-Dimethylfuran	+	+	+	+	–
12	C	96	2,4-Dimethylfuran	+	+	+	+	–
13	C	96	2,3-Dimethylfuran	+	+	+	+	–
14	C	94	2-Vinylfuran	+	+	+	+	–
15	A	84	Pent-3-en-2-one	+	+	+	+	–
16	A	82	1,4-Pentadiene-3-one	+	+	–	–	–
17	B	84	3(*H*)-Furan-3-one	+	+	+	–	–
18	C	110	2-Ethyl-5-methylfuran	+	+	+	+	–
19	D	94	1-Methyl-1,3-cyclohexadiene	+	+	+	–	–
20	D	94	1-Methyl-1,4-cyclohexadiene	+	+	+	–	–
21	D	92	Toluene	+	+	+	+	+
22	A	102	Pyruvic acid methyl ester	+	–	–	–	–
23	B	84	2*H*-Furan-3-one	+	+	+	–	–
24	B	96	3-Furaldehyde	+	+	–	–	–
25	A	82	2,4-Pentadienal	+	+	+	–	–
26	B	96	2-Furaldehyde	+	+	+	–	–
27	B	98	2-Methyl-(2*H*)-furan-3-one	+	–	–	–	–
28	A	100	4-Methyl-tetrahydrofuran-3-one	–	–	–	–	–
29	C	110	2,3,5-Trimethylfuran	+	+	+	+	–
30	C	108	2-Methyl-5-vinylfuran	+	+	+	+	–
31	C	110	2-Propylfuran	+	+	+	–	–
32	D	106	1,3-Dimethylbenzene	+	+	+	+	+
33	A	126	Furfuryl formate	–	–	–	–	–
34	D	106	1,4-Dimethylbenzene	+	+	+	+	+
35	D	104	Styrene	+	+	+	+	+
36	B	84	5*H*-Furan-2-one	+	+	+	–	–
37	A	96	2-Methyl-cyclopentene-1-one	+	+	+	–	–
38	D	106	1,2-Dimethylbenzene	+	+	+	+	+
39	B	110	2-Acetylfuran	+	+	+	+	–
40	B	110	3-Acetyl furan	–	–	–	–	–
41	A	98	2,3-Dihydro-5-methyl-furan-2-one	+	–	–	–	–
42	B	110	5-Methyl-2-furaldehyde	+	+	–	–	–
43	B	126	2-Acetyl-3-hydroxyfuran	–	–	–	–	–
44	D	120	Ethyltoluene	+	+	+	+	+
45	D	94	Phenol	+	+	+	+	+
46	D	120	Ethyltoluene	+	+	+	+	+
47	E	118	Benzofuran	+	+	+	+	+
48	E	118	Benzofuran	+	+	+	+	+

Table 1 (continued)

No.	Class	MW [a]	Compound [b]	Sample				
				1	2	3	4	5
49	D	120	Ethyltoluene	−	−	+	+	+
50	D	124	2-Methoxyphenol	+	+	−	−	−
51	A	112	Methyldihydropyranone	+	+	−	−	−
52	A	112	Methyldihydropyranone	+	+	−	−	−
53	D	122	Salicylaldehyde	+	+	+	−	−
54	A	112	3-Hydroxy-2-methyl-2-cyclopentene-1-one	−	−	−	−	−
55	E	116	1*H*-Indene	+	+	+	+	+
56	D	124	Methoxyphenol	+	+	−	−	−
57	E	134	3′-Methylacetophenone	+	+	+	+	−
58	D	108	2-Methylphenol	+	+	+	+	+
59	D	108	3-Methylphenol	+	+	+	+	+
60	D	108	4-Methylphenol	+	+	+	+	+
61	E	132	Methylbenzofuran	+	+	+	+	+
62	E	132	Methylbenzofuran	+	+	+	+	+
63	A	126	Levoglucosenone	+	−	−	−	−
64	A	126	3-Hydroxy-2-methyl-(4*H*)-pyranone	−	−	−	−	−
65	D	122	Dimethylphenol	+	+	+	+	−
66	E	132	Methylbenzofuran	+	+	+	+	+
67	E	134	2′-Methylacetophenone	+	+	+	+	−
68	A	144	5-Hydroxymethyl-2-tetrahydrohydro-furaldehyde	−	−	−	−	−
69	A	128	2-Hydroxymethyl-2,3-dihydro-4(*H*)-pyran-4-one	−	−	−	−	−
70	D	122	Dimethylphenol	+	+	+	+	−
71	D	122	Demethylphenol	+	+	+	+	−
72	E	130	2-Methyl-1*H*-indene	+	+	+	+	+
73	E	130	1-Methyl-1*H*-indene	+	+	+	+	+
74	D	122	Dimethylphenol	+	+	+	−	−
75	D	122	Dimethylphenol	+	+	+	−	−
76	E	128	Napthtalene	+	+	+	+	+
77	A	144	1,4:3,6-Dianhydro-D-glucopyranose	−	−	−	−	−
78	D	110	1,2-Dihydroxybenzene	+	−	−	−	−
79	E	146	Dimethylbenzofuran	+	+	+	+	+
80	E	146	Dimethylindene	+	+	+	+	+
81	E	146	Dimethylbenzofuran	+	+	+	+	+
82	D	124	Methylbenzenediol	+	+	−	−	−
83	A	144	1,4-Dideoxy-D-*glycero*-hexulose	−	−	−	−	−
84	D	158	Diisopropenylbenzene	+	+	+	+	−
85	E	142	1-Methylnaphtalene	+	+	+	+	+
86	E	142	2-Methylnaphtalene	+	+	+	+	+
87	E	156	1,8-Dimethylnaphtalene	+	+	+	+	+
88	E	156	1,3-Dimethylnaphtalene	+	+	+	+	+
89	E	144	1-Naphtalenol	+	+	+	+	+
90	E	144	2-Naphtalenol	+	+	+	+	+
91	E	168	Dibenzofuran	+	+	+	+	+
92	E	166	9*H*-Fluorene	+	+	+	+	+
93	E	182	2-Hydroxyfluorene	+	+	+	+	+
94	E	182	4-Methyl-dibenzofuran	+	+	+	+	+
95	E	180	4-Methyl-9*H*-fluorene	+	+	+	+	+
96	A	162	Levoglucosan	−	−	−	−	−

[a] A, sugar markers; B, functionalized furans; C, alkyl furans; D, benzenoid aromatics; and E, condensed aromatics.

[b] Identification based on EIMS spectra.

Table 2
Identified compounds in the Cu(770°C)-Py–GC–MS data of char (270) (1), char 290 (2), char 310 (3), char 350 (4), and char 390 (5). The numbering of the compounds corresponds with Fig. 2

No.	Class [a]	MW	Compound [b]	Sample					
				1	2	3	4	5	6
1	A	86	2,3-Butanedione	+	+	+	+	+	–
2	C	82	2 or 3-Methylfuran	+	+	+	+	+	+
3	A	70	2-Butenal (*cis*)	+	+	+	+	+	–
4	A	70	2-Butenal (*trans*)	+	+	+	+	+	–
5	A	74	Hydroxypropanone	+	+	+	+	–	–
6	D	80	1,4-Cyclohexadiene	–	–	+	+	+	+
7	D	80	1,3-Cyclohexadiene	–	–	+	+	+	+
8	D	78	Benzene	–	+	+	+	+	+
9	A	86	Tetrahydrofuran-3-one	+	+	+	+	+	–
10	C	96	2-Ethylfuran	–	–	+	+	+	+
11	C	96	2,5-Dimethylfuran	–	–	+	+	+	+
12	C	96	2,4-Dimethylfuran	–	–	+	+	+	+
13	C	96	2,3-Dimethylfuran	–	–	+	+	+	+
14	C	94	2-Vinylfuran	–	–	+	+	+	+
15	A	84	Pent-3-en-2-one	+	+	+	+	+	+
16	A	82	1,4-Pentadiene-3-one	+	+	+	+	+	+
17	B	84	3(*H*)-Furan-3-one	+	+	+	+	+	–
18	C	110	2-Ethyl-5-methylfuran	–	–	–	+	+	+
19	D	94	1-Methyl-1,3-cyclohexadiene	–	–	–	–	+	+
20	D	94	1-Methyl-1,4-cyclohexadiene	–	–	–	–	+	+
21	D	92	Toluene	–	+	+	+	+	+
22	A	102	Pyruvic acid methyl ester	+	+	+	+	+	–
23	B	84	2*H*-Furan-3-one	+	+	+	+	+	–
24	B	96	3-Furaldehyde	+	+	+	+	+	–
25	A	82	2,4-Pentadienal	+	+	+	+	+	–
26	B	96	2-Furaldehyde	+	+	+	+	+	–
27	B	98	2-Methyl-(*H*)-furan-3-one	+	+	+	+	+	–
28	A	100	4-Methyl-tetrahydrofuran-3-one	+	+	+	+	+	+
29	C	110	2,3,5-Trimethylfuran	–	–	–	+	+	+
30	C	108	2-Methyl-5-vinylfuran	–	–	+	+	+	+
31	C	110	2-Propylfuran	–	–	+	+	+	+
32	D	106	1,3-Dimethylbenzene	–	–	+	+	+	+
33	A	126	Furfuryl formate	+	+	+	–	–	–
34	D	106	1,4-Dimethylbenzene	–	–	+	+	+	+
35	D	104	Styrene	–	–	–	+	+	+
36	B	84	5*H*-Furan-2-one	+	+	+	+	+	+
37	A	96	2-Methyl-cyclopentene-1-one	–	–	+	+	+	–
38	D	106	1,2-Dimethylbenzene	–	–	–	+	+	+
39	B	110	2-Acetylfuran	–	+	+	+	+	+
40	B	110	3-Acetylfuran	–	+	+	+	+	–
41	A	98	2,3-Dihydro-5-methyl-furan-2-one	+	+	+	+	–	–
42	B	110	5-Methyl-2-furaldehyde	–	+	+	+	+	+
43	B	126	2-Acetyl-3-hydroxyfuran	–	–	–	+	+	–
44	D	120	Ethyltoluene	–	–	+	+	+	+

Table 2 (continued)

No.	Class [a]	MW	Compound [b]	Sample					
				1	2	3	4	5	6
45	D	94	Phenol	−	+	+	+	+	+
46	D	120	Ethyltoluene	−	−	−	+	+	+
47	E	118	Benzofuran	−	−	+	+	+	+
48	E	118	Benzofuran	−	−	−	+	+	+
49	D	120	Ethyltoluene	−	−	+	+	+	+
50	D	124	2-Methoxyphenol	−	−	−	+	+	+
51	A	112	Methyldihydropyranone	+	+	+	+	+	+
52	A	112	Methyldihydropyranone	+	+	+	+	+	+
53	D	122	Salicylaldehyde	−	−	−	+	+	+
54	A	112	3-Hydroxy-2-methyl-2-cyclopentene-1-one	+	+	+	+	+	+
55	E	116	1*H*-Indene	−	−	−	+	+	+
56	D	124	Methoxyphenol	−	−	−	+	+	+
57	E	134	3′-Methylacetophenone	−	−	−	+	+	+
58	D	108	2-Methylphenol	−	−	+	+	+	+
59	D	108	3-Methylphenol	−	−	+	+	+	+
60	D	108	4-Methylphenol	−	−	+	+	+	+
61	E	132	Methylbenzofuran	−	−	−	+	+	+
62	E	132	Methylbenzofuran	−	−	−	+	+	+
63	A	126	Levoglucosenone	+	+	+	+	+	−
64	A	126	3-Hydroxy-2-methyl-(4*H*)-pyranone	+	+	+	+	−	−
65	D	122	Dimethylphenol	−	−	−	+	+	+
66	E	132	Methylbenzofuran	−	−	−	+	+	+
67	E	134	2′-Methylacetophenone	−	−	−	+	+	+
68	A	128	2-Hydroxymethyl-2,3-dihydro-4(*H*)-pyran-4-one	+	+	+	+	−	−
69	A	144	5-Hydroxymethyl-2-tetrahydro-furaldehyde	+	+	+	+	−	−
70	D	122	Dimethylphenol	−	−	−	+	+	+
71	D	122	Dimethylphenol	−	−	−	+	+	+
72	E	130	2-Methyl-1*H*-indene	−	−	−	+	+	+
73	E	130	1-Methyl-1*H*-indene	−	−	−	+	+	+
74	D	122	Dimethylphenol	−	−	−	+	+	+
75	D	122	Dimethylphenol	−	−	−	+	+	+
76	E	128	Napthtalene	−	−	−	+	+	+
77	A	144	1,4:3,6-Dianhydro-D-glucopyranose	+	+	+	+	−	−
78	D	110	1,2-Dihydroxybenzene	+	+	+	+	+	−
79	E	146	Dimethylbenzofuran	−	−	−	+	+	+
80	E	146	Dimethylindene	−	−	−	+	+	+
81	E	146	Dimethylbenzofuran	−	−	−	+	+	+
82	D	124	Methylbenzenediol	−	−	+	+	+	+
83	A	144	1,4-Dideoxy-D-*glycero*-hexulose	+	+	+	+	−	−
84	E	132	1-Indanone	−	−	−	+	+	+
85	D	158	Diisopropenylbenzene	−	−	−	+	+	+
86	E	142	1-Methylnaphtalene	−	−	−	+	+	+
87	E	142	2-Methylnaphtalene	−	−	−	+	+	+
88	A	162	Levoglucosan	+	+	+	+	−	−

[a] A, sugar markers; B, functionalized furans; C, Alkyl furans; D, benzeoid aromatics; and E, condensed aromatics.

[b] Identification based on EIMS spectra.

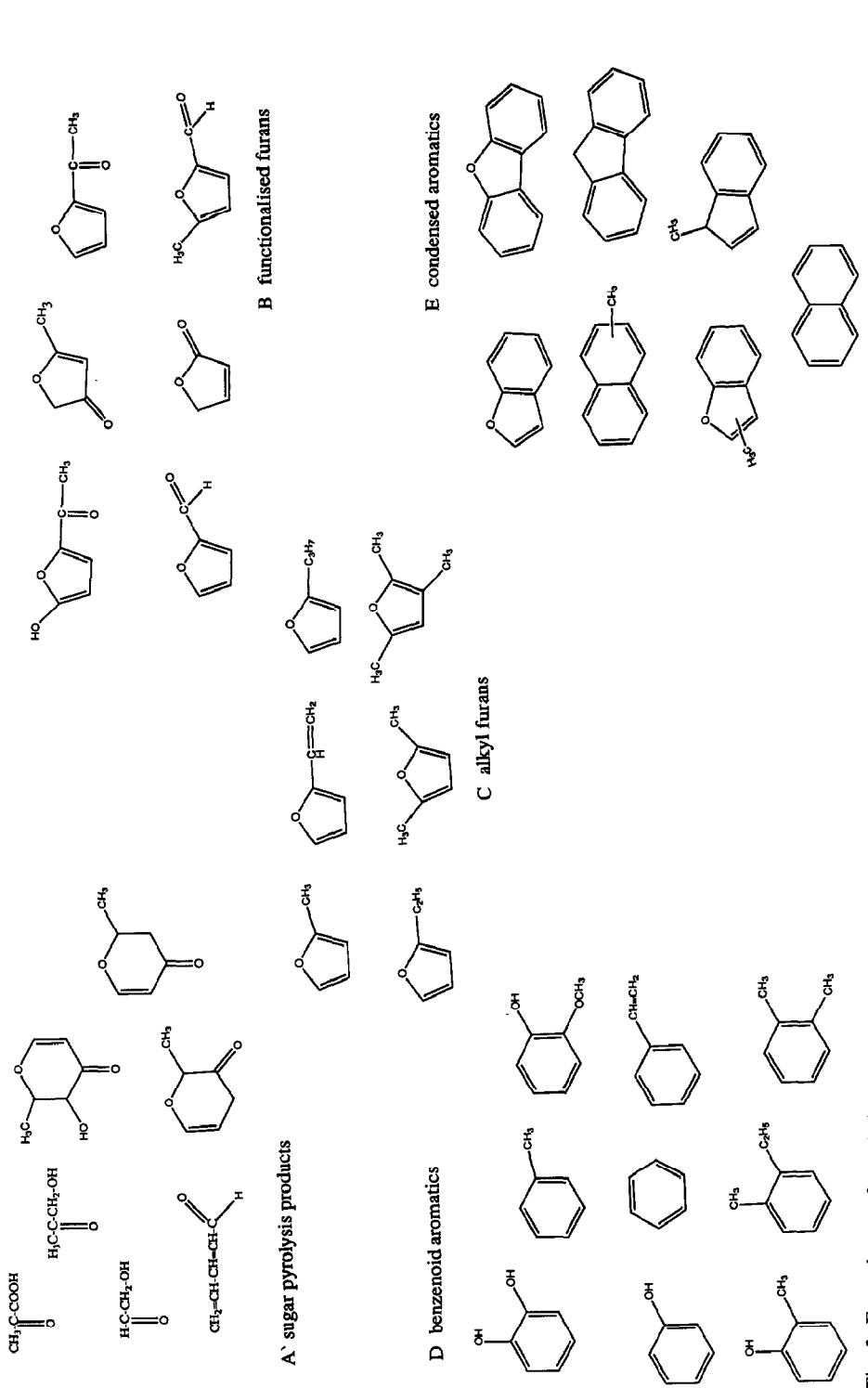

Fig. 3. Four classes of pyrolysis products from cellulose and cellulose chars: A, sugar markers; B, functionalized furans; C, alkyl furans; D, benzenoid aromatics; and E, condensed aromatics.

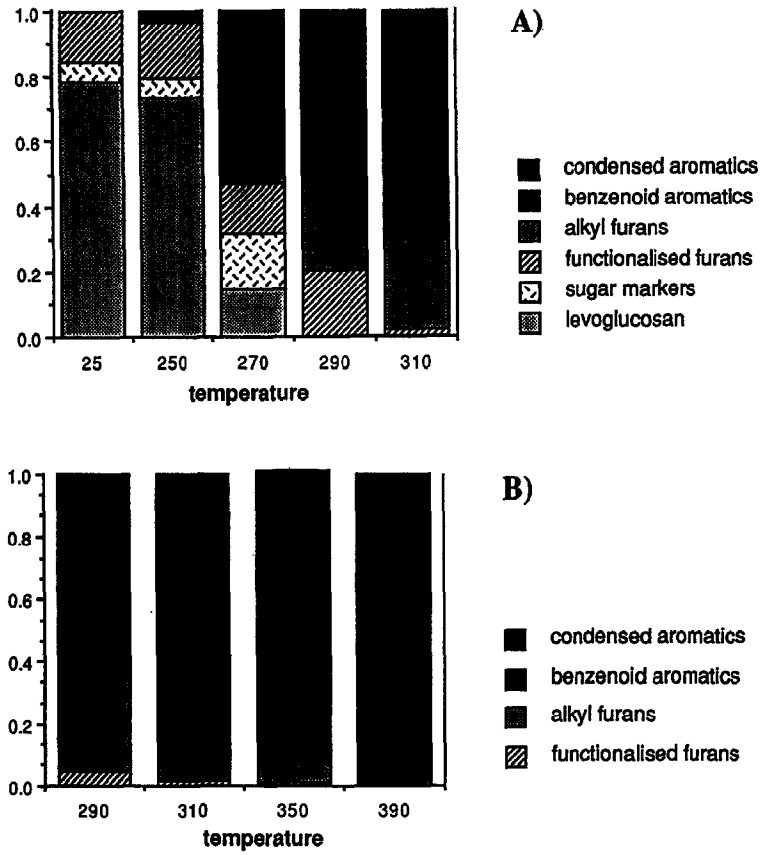

Fig. 4. Distribution of pyrolysis products with different charring temperatures in Cu-py–GC–MS data. A, 610°C Curie point and B, 770°C Curie point.

again implied by the ratio of intensities for the C = 0 and C = C bands in the spectra. The aromatic character of these two char residues is clear from the absorption bands at 750, 800, and 870 cm^{-1} (aromatic out of plane bending) and a broad absorption 1000–1200 cm^{-1} (C–H deformation vibrations in aromatics), typical for substituted aromatic rings such as benzene.

Nuclear magnetic resonance spectroscopy.—Solid-state CP/MAS ^{13}C NMR spectra of cellulose and several cellulose chars are presented in Fig. 3. The NMR spectrum of cellulose reveals several sharp resonance lines that are characteristic of crystalline cellulose. Chemical shifts are assigned as follows: C-6 is assigned to the asymmetric resonance at 65 ppm; C-2, C-3, and C-5 are assigned to the intense doublet centered at 73 ppm; C-4 is the asymmetric doublet centered at 85 ppm; and the anomeric carbon, C-1, appears as a sharp resonance at 105 ppm. The multiplicity of the resonance due to C-4 arises from site inequivalence in the unit cell that is induced by crystal packing. It has been shown previously that site symmetry of the lattice can be lower than the molecular symmetry, giving rise to

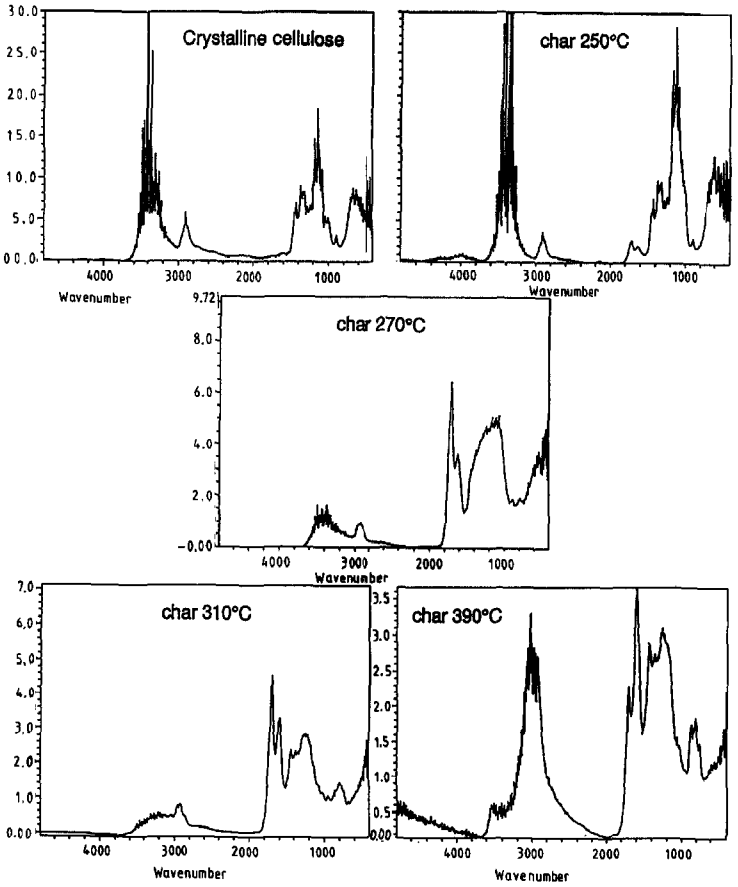

Fig. 5. FTIR spectra of microcrystalline cellulose and cellulose chars 250, 270, 310, and 390.

Table 3
Absorption bands in the FTIR spectra of microcrystalline cellulose and their assignment

Region (cm^{-1})	Assigned to
3100–3600	O–H (stretching)
2800–3000	C–H (stretching)
1410	CH_2 (bending)
1310–1360	C–C and C–O (skeletal vibrations)
1360	O–H (bending)
1200	C–O (stretching in pyranose ring)
1170	C–O (antisymetric bridge stretching)
1110	C–OH (skeletal vibrations)
1080	C–O–C (pyranose ring skeletal vibrations)
1030	C–O (C-6 skeletal vibrations)
990	C–O (secondary alkohols skeletal vibrations)

more than one resonance from some carbons in crystalline cellulose samples [24,25].

The NMR spectrum of char 220 (not shown) is essentially the same as that of cellulose. In addition to having slightly broadened resonance lines for cellulose carbons, the spectrum of char 250 exhibits three distinct resonances of low intensity in the carbonyl region at ca. 195, 202, and 209 ppm. The carbonyl resonances account for ca. 0.6% of the total integrated carbon signal in the spectrum, and are consistent with the appearance of small amounts of stable compounds such as unsaturated aldehydes (2,4-pentadienal), unsaturated cyclohexenones [3-hydroxy-2-methyl-2,3-dihydro-(4*H*)-pyran-4-one], and unsaturated cyclopentenones [2-methyl-(2*H*)-furan-3-one], respectively.

Pronounced changes can be seen in the spectra of chars 270 and 290 (not shown). One observes the appearance and growth of aromatic (100–155 ppm) and

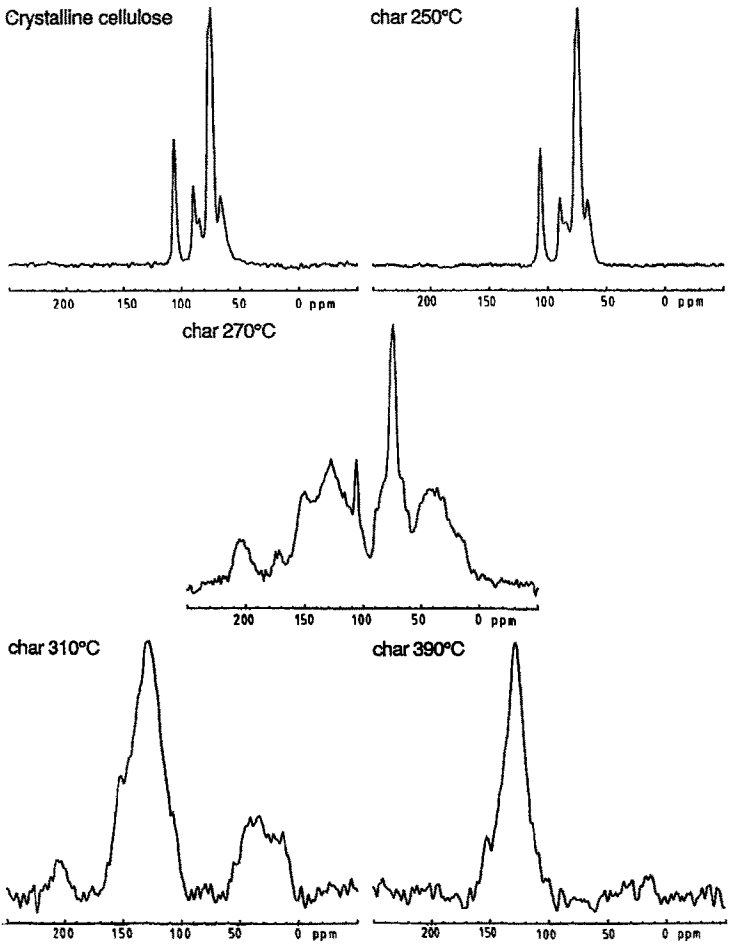

Fig. 6. Solid-state ^{13}C NMR spectra of microcrystalline cellulose and chars 250, 270, 310, and 390.

aliphatic (10–60 ppm) structures with increasing charring temperature. The presence of the resonance band at 155 ppm in the aromatic region is indicative of either furanyl or, possibly, phenolic C–O functionalities. Resonances centered at ca. 175 and 205 ppm are consistent with the formation of carbonyl functional groups; absorptions in the 175–180 ppm region may be consistent with either carboxylic acids or furaldehydes. On the other hand, a rapid decrease in the relative amounts of carbohydrate structures is observed in the spectra of these two chars. In char 270, a significant contribution from crystalline cellulose is evidenced by the sharp resonances at 75 and 105 ppm. However, the broad base of the resonance at 75 ppm suggests the formation of an amorphous cellulose component as well. The spectrum of char 290 indicates that a major portion of the ordered cellulose has been altered; only a broad amorphous component is evident.

Higher pyrolysis temperatures (310–390°C) result in more extensive structural rearrangement reactions. Changes observed in spectra of chars 310–390 reveal a progressive loss of oxygen functionality. There is a progressive loss of carbonyl absorptions at 205 ppm with increasing char temperature, until virtually all of the carbonyl groups are absent in char 390. Moreover, all of the furaldehyde structures (175 ppm) have been lost in char 310. The width of the aromatic absorption band narrows significantly due to loss of aromatic C–O absorptions at about 155 ppm, consistent with loss of furans. The aromatic character of the chars increases rapidly with temperature after char 310; the fraction carbon aromaticity of char 350 is 0.83, and this value increases to 0.93 for char 390.

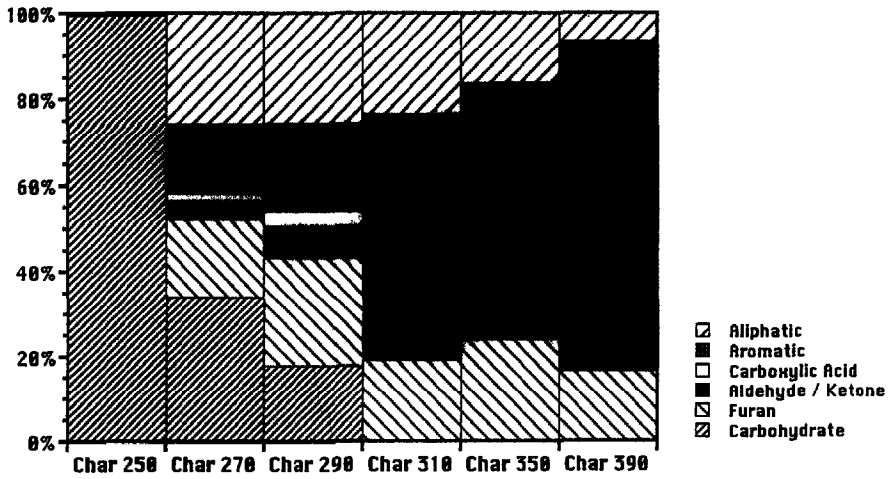

Fig. 7. Contribution of different functional groups to the total carbon distribution in solid-state ^{13}C NMR data of chars 250, 270, 290, 310, 350, and 390.

4. Discussion

NMR and FTIR have been used to verify the suitability of pyrolysis–gas chromatography–mass spectrometry for studying cellulose chars. These nondestructive spectroscopic methods provide an insight into the functional groups and type of bonds present in the chars themselves, and the preservation and the destruction of the glucan structure with the rising temperature can easily be monitored. Py–GC–MS offers a more detailed look at the different structures released from the chars, but it is possible that the Py–GC–MS data give a false image of the char structures since the original chemical bonds are disrupted and many rearrangement reactions may occur.

We can divide the heating process of cellulose into three stages. In Stage I, all three methods confirm the preservation of oligosaccharides in the chars up to a temperature of 270°C, as described earlier [14]. NMR also supports the idea that the preservation of oligosaccharides is closely linked with the preservation of crystallinity by the slow heating procedure [14] (Fig. 6). The NMR spectra of chars 220 and 250 still show an orderly glucan structure, and both the Py–MS [14,15] and Py–GC–MS (Table 1) product distribution of these chars are very similar, almost identical with that of native microcrystalline cellulose. However, the colour of the samples changed from the white of microcrystalline cellulose to yellow for char 220 and brown for char 250, indicating the presence of conjugated systems at local reaction sites. Indeed, FTIR of these chars shows that some unsaturated C–C bonds and carbonyl groups are formed in the cellulose, probably by elimination of water. Glucopyranose rings with unsaturated bonds may still be part of the cellulose macromolecule. In this way, amorphous centers are formed in the originally highly ordered cellulose [14].

Stage II begins around 250°C and continues towards higher temperatures. All three analytical methods used show quite a number of new elements in char 270. Py–MS of the acid hydrolysis residue of char 250 showed that these new elements are already present at this relatively low temperature. The table of pyrolysis products lists a number of furans with aliphatic side chains and a range of benzene and phenol derivatives. NMR and FTIR confirm that, while part of the glucan structure is still preserved in this sample, it clearly already contains a new intermediate polymer built of phenol and furan elements formed by rearrangement and condensation reactions. In the higher temperature chars the thermolabile carbohydrate moieties and furans decrease and gradually disappear (char 350) (Figs. 4 and 7). On the other hand, the increase of aromatic and condensed aromatic compounds was detected by all three analytical methods (Stage III).

The destruction of the glucan structure and the chemical changes can be seen by a relative quantification of the pyrolysis products and their distribution. For simplicity, the pyrolysis products in Py–GC–MS have been divided into five classes (Fig. 3A–E). Their contribution to the total product distribution is shown in Fig. 4A and B. Although these compounds are analytical pyrolysis products of the chars, comparing these results with a similar quantification from the NMR measurements (Fig. 7) makes it clear that a number of furan and aromatic compounds

are present in the char itself, trapped in the 3D structure of the newly formed polymer or chemically bound to the altered cellulose. Although the response factor of individual compounds was not taken into consideration for the Py–GC–MS

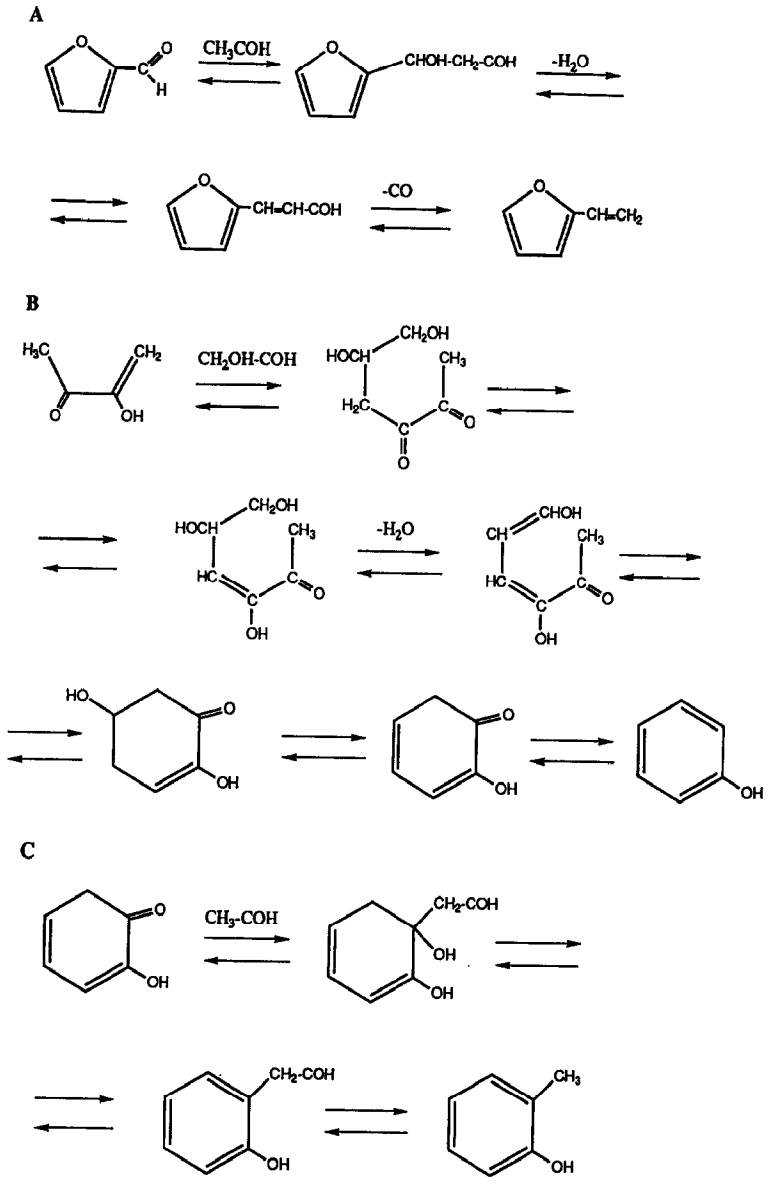

Scheme 1. Proposed reaction pathways of some compounds, identified among the pyrolysis products of cellulose chars.

relative quantification, there is a striking resemblance between the results obtained by Py–GC–MS and ^{13}C NMR, the same trends being seen by both methods.

Py–GC–MS offers a more detailed look at the different structures released from the chars and, therefore, suggests some processes that are taking place during the preparation of the chars from microcrystalline cellulose. New bonds seem to be formed by condensation reactions of primary pyrolysis products of cellulose in the amorphous regions, as crystalline regions are said to be the main source of levoglucosan. At atmospheric pressure, the primary reaction products are less volatile than under vacuum conditions, and hence more subject to secondary pyrolysis reactions in the pyrolysis furnace. "Wet" chemistry of carbohydrates shows that base catalysed aldol reactions are the main pathway for the formation of aromatic compounds. Aldol and retro-aldol reactions, normally catalysed by acids or bases, do occur as a thermal process [26]. Relatively weak bases promote the condensation of β-diketones with aldehydes [27]. All these reactions lead to conjugated unsaturated aldehydes, which can decarbonylate under high temperatures. Whether the decarbonylation step occurs during the preparation of the chars or during the Curie-point analytical pyrolysis is open to question. It was shown previously that cinnamaldehyde, upon being heated at 360°C with Raney Ni, gave carbon monoxide, styrene, ethylbenzene, toluene, and benzene. A similar product distribution was obtained by passing cinnamaldehyde through a hot tube [28]. In our case, the pyrolysis wire during the Py–GC–MS or Py–MS analysis can act as the catalyst. 2-Methylfuran, furan, and especially 2-ethylfuran, 2-vinylfuran, ethylbenzene, toluene, and styrene appear in the pyrolysates of the chars from chars 250 to 350. Therefore, we assume that cinnamaldehyde and the furan analogue 3-(2-furyl)-propenal are present in these chars.

Some possible reactions are shown in Scheme 1. The starting point are always compounds that have been previously identified in pyrolysates of cellulose like furfural, acetaldehyde (Scheme 1A and C), and 2,3-butanedione or 2-hydroxyacetaldehyde (Scheme 1B). Minor amounts of dihydroxybenzene and methylphenols have been found in pyrolysates of microcrystalline cellulose [22], and we

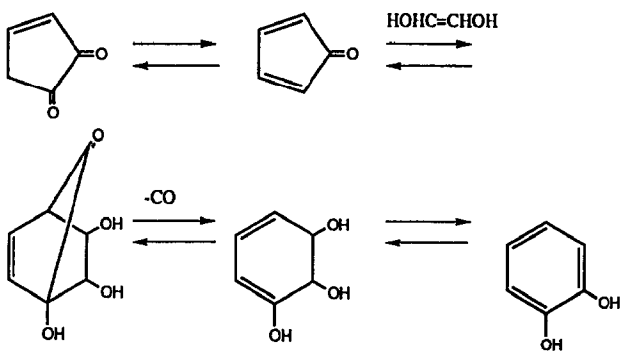

Scheme 2. Proposed reaction pathway for formation of dihydroxy benzene, identified in pyrolysates of both microcrystalline cellulose and cellulose chars.

believe that they are products of secondary pyrolysis reactions, which were enhanced in our case. The range of isomers of methyl aromatic compounds (methyl phenols, dimethyl benzenes, and phenols, methyl benzofurans, and indenes, etc.) can be explained by radical reactions during the Curie-point Py–GC analysis. With heating at higher temperatures during the preparation of chars, this process might occur in the solid residues themselves.

Another type of reaction that may be responsible for the formation of the condensed char are Diels–Alder type reactions [28,29] (Scheme 2).

Based on all these analytical results, we propose a model for the formation of the intermediate temperature chars. Amorphous, disordered glucan chains are the source of small volatile compounds such as enolic furans, glycolaldehyde, butanedione, ketene, etc. We postulate that residual nonvolatile, perhaps anhydroglucose chains with ring cleavage products like acetaldehyde attached to O–C-4 and O–C-1 act as aldol condensation sites for the smaller reactive molecules (Scheme 2). The result is a rapidly growing three-dimensional network polymer, which continuously grows by trapping small reactive pyrolysis products while reacting with the larger residual glucan residues. The growth of this polymer is analogical to the growth of a dendrimer polymer, in which reactive functional groups of a monomer or an oligomer condense with small reactive molecules to form a three-dimensional polymer [30,31]. For microcrystalline cellulose, this process begins at temperatures around 250°C (Stages II and III). In char 250, it is possible to detect preserved cellulose structure and at the same time the furan–phenol polymer is formed. The growth rate increases dramatically at incubation temperatures above 250°C. The newly formed, thermally stable polymer system dissociates further at temperatures above 310°C, by homolytic cleavage reactions [32], and condenses further by radical reactions [5] into a polyaromatic structure.

5. Summary

There is an excellent correlation between the data from Py–GC–MS, NMR, and FTIR. NMR supports the preservation of β-(1 → 4)-glucan chains in a crystalline or highly ordered state up to 250°C, as proposed earlier [14]. At 250°C and higher, cellulose changes into a new polymer. This polymer has furanoid skeletons, hydroxyaromatic skeletons, unsaturated hydrocarbon chains, and a high number of carboxyl and carbonyl groups. With increasing temperature, further dehydration occurs and at $t > 310$°C disproportionation occurs by loss of CO and CO_2 leading to a highly condensed aromatic polymer.

Acknowledgements

The research program on the Mass Spectrometry of Macromolecular Systems is part of the research program of FOM (Foundation for Fundamental Research on Matter), a subsidiary of the Dutch Organisation for Scientific Research (NWO).

The technical help of J.B.M. Pureveen and G.B. Eijkel at FOM is gratefully acknowledged. R.E. Botto gratefully acknowledges support from the Office of Basic Energy Sciences, Division of Chemical Sciences, U.S. Department of Energy, under contract no. W-31-109-ENG-38.

References

[1] M.J. Antal, Jr., *Am. Solar Energy Soc.*, (1983) 61–111.
[2] F. Shafizadeh, *Adv. Carbohydr. Chem. Biochem.*, 23 (1968) 419–474.
[3] F. Shafizadeh and A.G.W. Bradbury, *J. Appl. Poly. Sci.*, 23 (1979) 1431–1442.
[4] D. Radlein, J. Piskorz, and D.S. Scott, *J. Anal. Appl. Pyrolysis*, 19 (1991) 41–63.
[5] F. Shafizadeh, *J. Anal. Appl. Pyrolysis*, 3 (1982) 283–305.
[6] F.J. Kilzer and A. Broido, *Pyrodynamics*, 2 (1965) 151–163.
[7] J.A. Lomax, J.M. Commandeur, P.W. Arisz, and J.J. Boon, *J. Anal. Appl. Pyrolysis*, 19 (1991) 65–80.
[8] M.M. Tang and R. Bacon, *Carbon*, 2 (1964) 211–220.
[9] C. Morterra, M.J.D. Low, and A.G. Severdia, *Carbon*, 22 (1984) 5–12.
[10] R.A. Friedel, J.A. Queiser, and H.L. Retkofsky, *J. Phys. Chem.*, 74 (1970) 908–912.
[11] Y.Z. Lai and F. Shafizadeh, *Carbohydr. Res.*, 38 (1974) 177.
[12] F. Shafizadeh, *Appl. Polym. Symp.*, 28 (1975) 153–174.
[13] D.F. Arseneau, *Can. J. Chem.*, 49 (1971) 632.
[14] I. Pastorova, P.W. Arisz, and J.J. Boon, *Carbohydr. Res.*, 248 (1993) 151–165.
[15] I. Pastorova, T.F.M. Oudemans, and J.J. Boon, *J. Anal. Appl. Pyrolysis*, 25 (1993) 63–75.
[16] T.F.M. Oudemans and J.J. Boon, *J. Anal. Appl. Pyrolysis*, 20 (1991) 197–228.
[17] T.F.M. Oudemans, J.J. Boon, and R.P. Evershed, *Proc. Third Natl. Conf. Archaeological Sci.*, 2–4 September 1991, York, UK, in press.
[18] M. Aho, P. Kortelainen, J. Rantanten, V. Linna, *J. Anal. Appl. Pyrolysis*, 15 (1989) 297–306.
[19] J.V. Ibarra and R. Moliner, *J. Anal. Appl. Pyrolysis*, 20 (1991) 171–184.
[20] S. Julien, E. Chornet, P.K. Tiwari, and R.P. Overend, *J. Anal. Appl. Pyrolysis*, 19 (1991) 81–104.
[21] J.V. Muntean, L.M. Stock, and R.E. Botto, *J. Magn. Reson.*, 76 (1988) 540–542.
[22] A.D. Pouwels, G.B. Eikel, and J.J. Boon, *J. Anal. Appl. Pyrolysis*, 15 (1989) 71–84.
[23] P.J.J. Tromp, J.A. Moulijn, and J.J. Boon, *Fuel*, 65 (1986) 960–967.
[24] R.H. Atalla, J.C. Gast, D.W. Sindorf, V.J. Bartuska, and G.E. Maciel, *J. Am. Chem. Soc.*, 102 (1980) 3249–51.
[25] W.L. Earl and D.L. Vanderhart, *J. Am. Chem. Soc.*, 102 (1980) 3251–52.
[26] R. Block, P.L. Perchec, F. Rousseac, and J.M. Coria, *Tetrahedron*, 24 (1968) 5971–5976.
[27] R.L. Reeves, in S. Patai (Ed.), *The Chemistry of Carbonyl Groups*, Interscience, New York, 1972, pp 567–620.
[28] W.M. Schubert and R.R. Kitner, in S. Patai (Ed.), *The Chemistry of Carbonyl Groups*, Interscience, New York, 1972, pp 696–760.
[29] Ogliaruso, Romanelli, and Becker, *Chem. Rev.*, 65 (1965) 261–367.
[30] A.W. van der Made, P.W.N.M. van Leeuwen, J.C. de Wilde, and R.A.C Brandes, *Adv. Mater.*, 5 (1993) 466–468.
[31] R. Engel, *Polym. News*, 17 (1992) 301–305.
[32] F. Shafizadeh and P.P.S. Chin, *Carbohydr. Res.*, 46 (1976) 149–154.